

The effect of lenslet resolution on the accuracy of ocular wavefront measurements

D.R. Neal, D. M. Topa and James Copland
WaveFront Sciences, Inc.
14810 Central Ave SE
Albuquerque, NM 87123-3905

The most critical element in a ocular Shack-Hartmann wavefront sensor is the micro-optic lenslet array. This array largely determines the accuracy of the wavefront measurement and the dynamic range of the measurements. This paper discusses the details of how the density of the lenslet array affects the accuracy of the wavefront measurement. We briefly discuss wavefront reconstruction, which is the mathematical process that takes the output from the lenslet array and reconstructs the input wavefront. We compare the two primary methods of reconstruction, the zonal fit and the modal fit. We also show how a denser array can be designed to have a better dynamic range.

1. Introduction

The use of wavefront sensors to measure ocular errors is a rapidly advancing field.¹ The ability of a clinician to measure, not just the basic refraction (sphere and cylinder) of a patient, but to obtain a spatially resolved map of the wavefront has opened up new possibilities for diagnosis and treatment.² These measurements, while introduced for adaptive optic retinoscopy³ are currently being applied to higher order LASIK and PRK corrections.⁴

In order to design the appropriate ocular system, the resolution of the measurement must be considered. In previous work relatively low resolution systems were chosen because adaptive optics systems had been low resolution.³ This minimized the computational load on computer. For even a 3 Hz closed-loop correction bandwidth, frames need to be acquired and analyzed at 30 Hz. Thus minimizing the number of focal spots needed was desirable.

In addition, for an adaptive optics system, the dynamic range is not a tremendous issue. In adaptive optics the deformable mirror is adjusted to minimize the optical figure errors and the current technologies for deformable mirrors all have limited dynamic range. In adaptive optic systems there was no reason to build a wavefront sensor with much more dynamic range than the deformable mirror. Thus each lenslet does not have to have a large dynamic range. The accuracy of the system depends upon the gain, or sensitivity, of the wavefront sensor, and the dynamic range depends upon the deformable mirror.

For a pure measurement system for eyes, however, the design point becomes somewhat different. There are no bandwidth concerns limiting the number of spots to consider and there is no deformable mirror to limit the dynamic range of interest. In fact with eyes each lenslet must have sufficient dynamic range to make an accurate measurement of the light incident upon it. It may be supposed that a large lenslet would have larger dynamic range. As we will show in this paper, this is not necessarily the case.

2. The Shack-Hartmann wavefront sensor

An ophthalmic wavefront measuring system consists of an imaging system, a means for injecting light into the eye, a wavefront sensor, and the various mounts, electronics, targets and cameras needed to make a practical system. While there are several types of systems currently in development, we will consider the types based on the Shack-Hartman wavefront sensing principle.

The Shack-Hartmann wavefront sensor⁵ is based on the principles of elementary optics. This is a well established field, with a variety of existing sensors that have been designed for many different applications.⁶ An input wavefront is projected through a lenslet array. The lenslets focus the light onto a CCD array. At the focal plane the output from each lenslet is a

small focal spot. The position of the focal spot is defined by the physical location of the peak and provides valuable information about the sampled portion of the wavefront.

Figure 1.1 below shows the output from nine lenslets. For example, WaveFront Sciences' Complete Ophthalmic Analysis System (COAS) has a 44×33 lenslet array for a total of 1,452 lenslets with each being a square of $144 \mu\text{m}$. The diameter of a human hair is approximately $100 \mu\text{m}$. The total array is $6.5 \times 4.8 \text{ mm}$.

If the wavefront over the lenslet is exactly planar, the intensity profile of the focal spot will be proportional to the ideal $\text{sinc}^2(x)\text{sinc}^2(y)$ function. This profile is shown in figure 1.2 (a). If the wavefront has mild aberrations the intensity profile will closely resemble the ideal focal spot. If the wavefront over the lenslet has significant aberrations, the focal spot will spread out and its position will be difficult to characterize. An example is shown in part (b) of the same figure.

The position of the focal spot contains clues about the shape of the wavefront over the lenslet. By measuring the positions of several focal spots we can determine the shape of the incident wavefront. The incident wavefront totally describes all the aberrations introduced by the complete optical system of the eye, from the retina through the cornea. So by measuring the positions of many focal spots, we can fully characterize the aberrations induced by the optical system and determine an extremely precise correction.

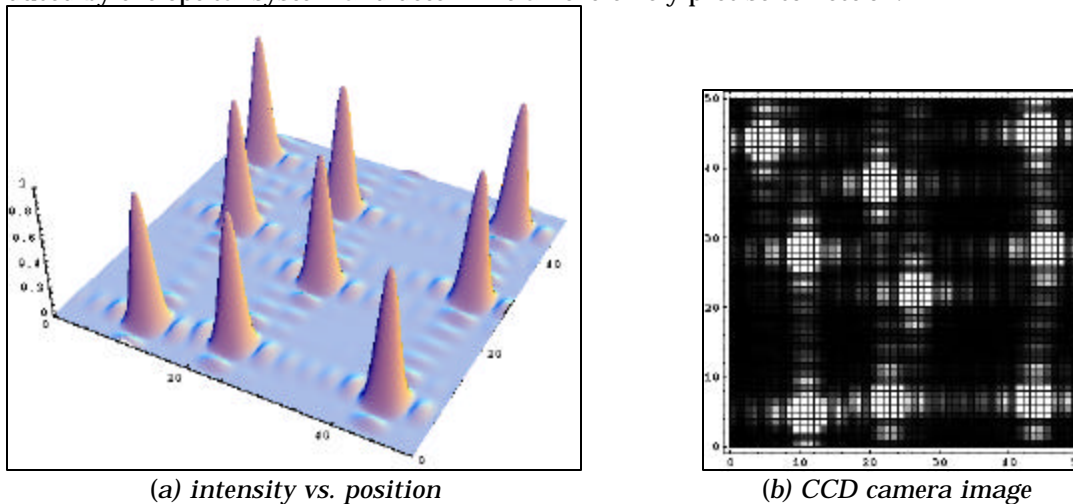


Figure 2.1: Lenslet output. This shows the output from nine micro-optic lenslets in the array. Part (a) shows the normalized intensity as a function of position. Each peak represents the output from a specific lens. The location of the peak is related to the slope of the wavefront averaged over the lenslet. The next part (b) shows how the CCD camera would record this display. The x and y axes in both parts are in units of CCD camera pixels.

The shift d_x in the position of the focal spot along the x axis is related to the average slope by

$$d_x = f \frac{q_x}{\sqrt{1+q_x^2}} \quad 1.$$

where f is the focal length of the lenslet and q_x is the average of the x slope of the wavefront. The shift d_y is defined similarly using q_y . For COAS, the focal length is 4.2 mm. For measurements of practical interest, the slope measurements are so small that $\sqrt{1+q_x^2}$ is indistinguishable from unity and it is very accurate to write

$$d_x = fq_x. \quad 2.$$

So the shift in the focal spot measures the average slope of the wavefront over the lenslet.

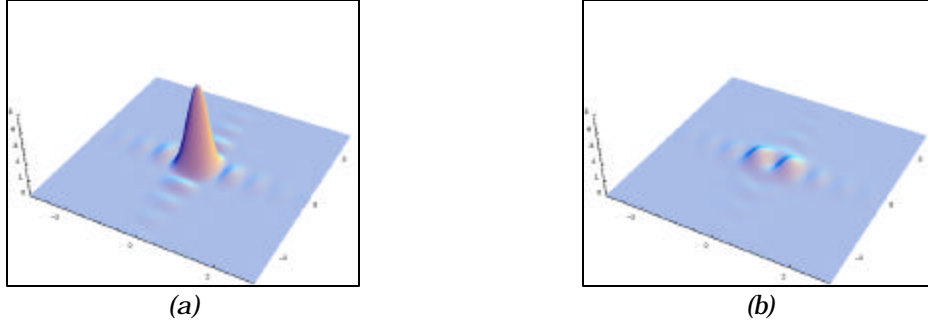


Figure 2.2: Ideal focus compared to a poor focus. When the wavefront sampled by the lenslet is nearly planar, the lenslet will produce the ideal focal spot show in part (a). Note how the light is strongly concentrated and the location of the peak is well-defined. In part (b), the sampled wavefront has a non-planar structure and the lenslet scatters light over a large region causing a diffuse and irregular focal spot. Characterizing the location of this focal spot is ambiguous at best.

Consider an arbitrary wavefront $y(x, y)$. The average x slope over a lenslet is defined by

$$q_x = \frac{\iint \frac{\partial y}{\partial x} dx dy}{d^2} \quad 3.$$

where d is the width of the lenslet. So the lenslet array reduces the entire structure of the sampled wavefront down to average slopes. In a quality wavefront sensor, the lenslet density will be so fine that over the region the size of any individual lenslet, the incident wavefront is highly planar. This is comparable to thinking of the sampled wavefront as a plane with only tip and tilt.

3. Focal spot degradation

The wavefront sensor detector only sees a pattern of focal spots. The position of these focal spots can be measured to extract the spatial derivatives of the wavefront at each lenslet. These derivatives are used to reconstruct the input wavefront.

If the position of these focal spots cannot be determined accurately the entire accuracy of the device will suffer. The light from each lenslet is incident upon a detector array, such as a CCD. Thus the focal spot is sampled by a fixed number of pixels and then digitized for storage in a computer. The digital image is broken up into a number of Areas of Interest (AOIs), with one focal spot in each AOI. These AOIs can then be processed to determine the position of the spot using the appropriate algorithm. For example, the thresholded centroid algorithm has been shown to have accuracy of a fraction of a pixel when the spot covers several pixels.^{5,6} That is:

$$r_x = \frac{\sum_i S_i x_i}{\sum_i S_i} \quad 4.$$

In order for the centroid to be accurately determined, the light incident on the detector must form a distinct grid of spots. To this end, the lenslet must sample a portion of the light that has low enough aberrations to form a detectable focal spot. Consider Figure 1.2. In case (a), a perfect flat wavefront, although with arbitrary tilt, was incident upon the lenslet array. It produces a sinc^2 pattern on the detector. This can readily be thresholded, sampled and digitized. The centroid algorithm will produced accurate, repeatable measurements of the spot location. In case (b), however, the incident light had a degraded wavefront. In this case the focal spot peak intensity is reduced and the spot is significantly blurred and spread out. The centroid algorithm may not be able to determine a spot position in this case at all.

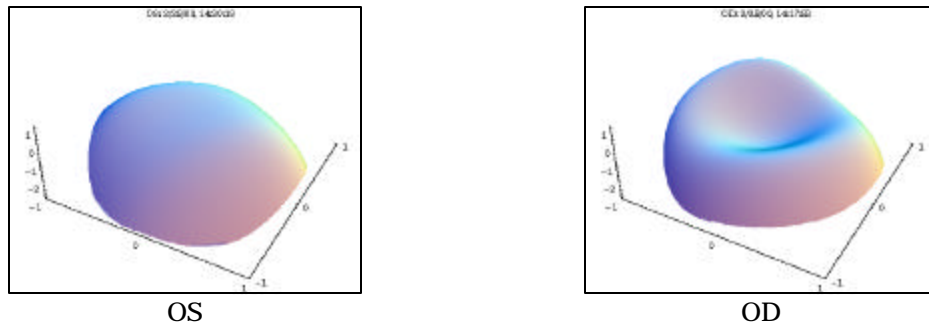


Figure 3.1: Sample wavefronts from a post-LASIK patient. These are the wavefronts as they exit the cornea and were measured one week after LASIK. The wavefront from the left eye has a simple structure but the wavefront on the right eye has a strong 3rd order spherical aberration. This causes a sharp drop off at the edge.

An algorithm that is optimized to accurately measure the location of a distinct spot will perform poorly on blurry spots. Conversely, an algorithm that can measure locations of blurry spots will not be the optimal one for measuring distinct spots. The best overall system then, will be one that optically makes each spot distinct. The way this is achieved is to use as many lenslets as possible over a given wavefront so that the wavefront is planar over each lenslet.

However, there is an obvious limit when a lenslet is too small. Then it covers too few CCD pixels to allow for accurate calculations of the spot location. The optimal balance between too big or too small a lenslet depends on the particular wavefronts that are to be measured. Computer simulations can determine the optimal balance for the wavefronts for measuring the human eye.

The wavefront sensor makes the inherent assumption that the incident wavefront is well modeled by a piecewise plane approximation. Thus, the precision of a wavefront sensor can be judged by comparing how well a sampled region resembles a plane. To explore this idea, we first present two sample wavefronts measured in the same post-LASIK patient as shown below. The left eye has a slowly varying structure and can be easily approximated as a series of planes, particularly if one was able to use 785 elements as in COAS. In this case using a lower lenslet density and fewer sample points would still give a reasonable result given the planarity of this wavefront.

The wavefront from the right eye shows the need for a high-density lenslet array to precisely measure the large curvature. This figure cannot be approximated reasonably with a small number of planar elements.

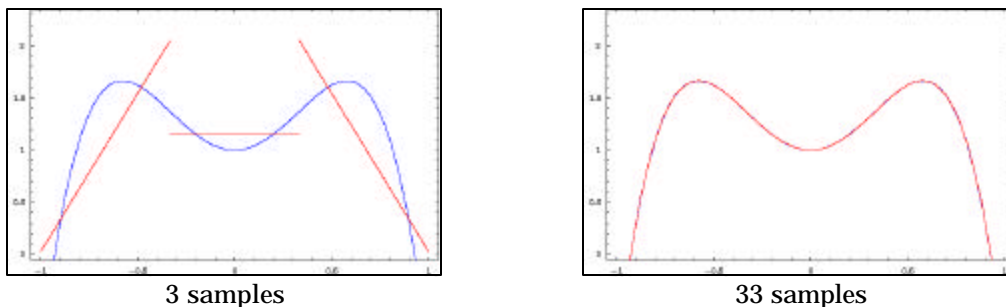


Figure 3.2: Planar approximation of a wavefront in two dimensions. A slice of the OD wavefront from figure 1.3 is studied here at two sample densities. The blue curve is the input wavefront; the red lines are the planar approximations made by the lenslet. For low sample densities, the wavefront is not approximated very well. For high sample densities the approximation is quite good.

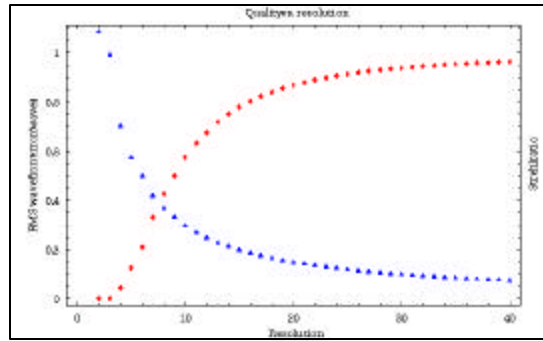


Figure 3.3: Quality as a function of lenslet density. The sample wavefront shown in the previous figure was used as an input function. The planar approximation was compared to the input wavefront by computing the root mean square of the difference between the blue and the red lines across each sample. Here the blue dots show this RMS error in waves; the red triangles show the corresponding value for the Strehl intensity.

To amplify this point, we have sliced the wavefront along the x axis to study the problem in two dimensions. We then resolved the curve into three linear elements and then 33 linear elements as shown below. The first case is an extremely crude approximation whereas the second is an excellent approximation. It is difficult to distinguish any separation between the blue input curve and the red approximation curve.

To quantify the approximation, we measured the square of the difference between the red and blue curves and computed the root mean square (RMS). This is the residual RMS wavefront error. One sees a dramatic decrease early on as the resolution or lenslet density increases. The improvement then begins to slow down. Adding a few lenses to an already dense array does not improve the wavefront error significantly. (But it does increase pixelation errors in determining the focal spot locations.)

The blue points of Figure 3.3 shows the residual RMS wavefront error for each of the lenslets in the array. This is sometimes referred to as the fitting error, or planar approximation error. The Strehl intensity can be shown⁷ to be reduced as a function of this value. The Strehl intensity is given as:

$$SR = e^{-\left(\frac{2\pi f_{rms}}{\lambda}\right)^2} \quad 5.$$

Figure 3.3 also shows the resulting Strehl ratio as a function of the lenslet resolution. It is clear that low resolution wavefront sensing results in poor Strehl intensity.

Since the eye is sometimes a very aberrated optical system, it is possible to design a wavefront measuring system that exhibits some of these effects.

For this paper a normal eye is defined as one that has weak higher order or high spatial frequency aberrations. A normal eye would have good Best Corrected Visual Acuity (BCVA), but not necessarily good uncorrected vision. For a normal eye, it is possible to obtain good focal spot images with even very low resolution systems.

In Figure 3.5, a similar image is presented from a wavefront sensor system with half the resolution. In this case, the images are also good clear images. The focal spots are well formed and their locations can be easily determined.

Figure 3.6 is an image from a high resolution wavefront of a RK eye. In this case, the physician attempted to correct for a large cylinder component in the original vision. In this case the surgery did not produce the desired result, and the resulting vision, both UCVA and BCVA is poor. In this image there are large regions near the edge where the light is scattered significantly. Light from these regions does not hit the wavefront sensor. These regions show up as dark in this image. However, examination of the focal spots reveals that these each has a well formed, precise image. In each case the focal spot position can be readily determined and the wavefront accurately measured, *in spite of extremely large aberrations.*



Figure 3.4: Normal eye, high resolution. The sample wavefront shown in the previous figure was used as an input function. The pupil in this case was 3.8 mm, with effective 210 μm resolution lenslets. The eye had a prescription of $-3.75 -1.00 \times 16$. The first figure shows the image of the full eye, the second figure zooms in on four focal spots.

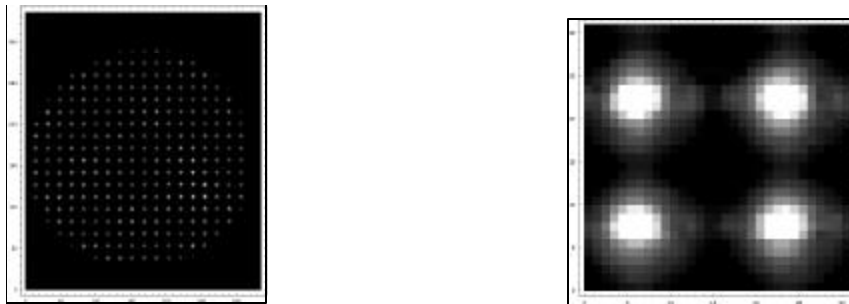


Figure 3.5: Normal eye, moderate resolution. This is an example of wavefront image from a normal eye. The pupil in this case was 6.8 mm, with 400 μm resolution lenslets. Note that these lenslets have much higher Fresnel numbers (shorter focal lengths compared to the higher resolution lenslets). This is the ratio of the focal spot separation to the spot radius.



Figure 3.6: RK eye, high resolution. This image was from an RK patient with very bad lateral, non-symmetrical cuts. While the cuts did not protrude into the optical zone, the resulting wavefront is seriously aberrated. The pupil in this case was 4.8 mm, with effective 210 μm resolution lenslets. Note that the focal spots are still extremely well formed and precise, even for this highly aberrated input wavefront.

By contrast, consider Figure 3.6 which is a measurement of an eye with kerataconus. In this case the resolution was 400 μm (instead of 210 μm). Each focal spot is significantly degraded and blurry. In places the focal spots are hard to even pick out. The region near the center, which is of the most interest, is not measurable at all.

Clearly a high resolution wavefront sensor produces better focal spots overall. This has the effect of making better measurements throughout the pupil, even in cases with extremely large aberration.

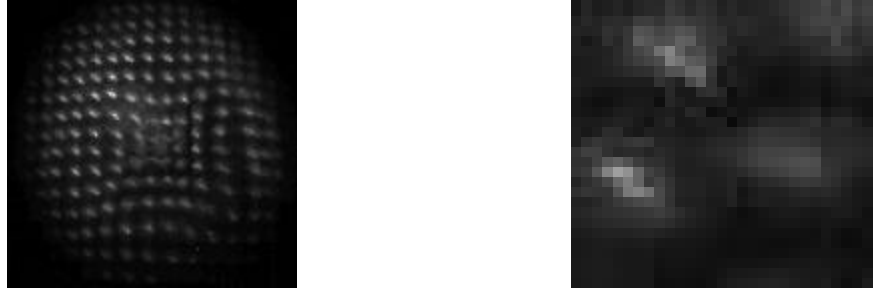


Figure 3.6: Kerataconus eye. This is an example wavefront from a eye with Kerataconus. The focal spots are extremely blurry and indistinct. From Thibos and Hong, OVS, Dec. 1999.

The drawback to the increased resolution is that more light that must be injected into the eye. If there are many more samples, then clearly the light that is reflected from the retina must be divided between many more lenslets.

Resolution (7 mm pupil)	Focal spots	Lenslet area (μm)	Power (μW)
33×33	800	210×210	22
18×18	254	400×400	6
10×10	78	700×700	2

Table 1. Power requirements for several different lenslet resolutions.

Each lenslet gets a correspondingly smaller fraction. However, as shown in Table 1, the effect is not so dramatic, with very reasonable and safe light levels needed, even for very high resolution systems. (The power level is based on injected light at 830 nm. More light is needed for visible wavelengths because of more efficient absorption by the eye.)

4. Wavefront reconstruction

Once the focal spot positions have been determined, the spatial derivatives are found using equation 2. The shift in focal spot is computed by using a reference that is recorded in a calibration step, and subtracting the reference location from each measured focal spot position.

Once the gradient map is known, the wavefront must be determined through some form of spatial integration. This step is called wavefront reconstruction⁸. There are two basic types of reconstructor: Zonal and Modal. The Zonal reconstructor directly numerically integrates the slope values to produce a wavefront map. Usually this produces very high resolution wavefront or OPD map. For COAS, this would be a set of 1,452 numbers. This type of reconstructor is generally very fast and accurate. The drawback is that a zonal reconstructor does not produce any overall information about the wavefront. While the wavefront map is very detailed, a further step is needed to calculate the sphere and cylinder or other terms. Sample output from these two types of reconstructors is shown in figure 4.1.

The Modal reconstructor, instead of numerically integrating the data at each point, fits the data to modes or polynomials. This allows direct extraction of important parameters, such as focus and astigmatism terms, along with other higher order coefficients. Modal reconstructors produce a set of coefficients that describe the wavefront in some arbitrary set of basis functions. A popular set of functions are the Zernike polynomials.⁹ Fitting a wavefront to 4th order Zernike polynomials would generate a set of 15 numbers. The output from a modal constructor is much more compact, but also less detailed. This compact notation makes it easy to compare results among different patients.

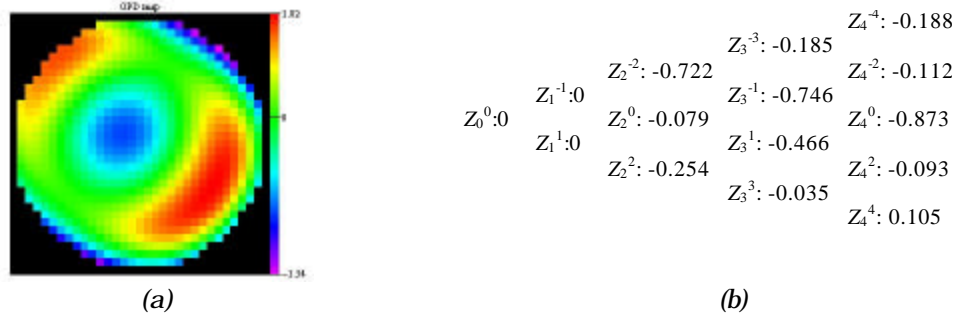


Figure 4.1 The output from the two types of wavefront reconstruction algorithms. Part (a) shows an OPD map created by a zonal reconstructor. The output from a modal reconstructor is shown in part (b). The zonal reconstructor is computationally more intensive than the modal reconstructor.

Often the modal wavefront reconstructor is used for expediency in computation and facility of comparison. If the same family of expansion functions is used in different measurements, the results can be compared. The ophthalmic community has followed the lead of the optics community and uses the Zernike polynomials in the modal reconstruction because the Zernike polynomials are closely related to functions that are commonly used to describe the primary aberrations of an optical system. The wavefront map is produced from the series expansion:

$$y(x, y) = \sum c_n^{-n} Z_n^{-n}(x, y). \quad 6.$$

When using the Zernike polynomials the sphere, cylinder and axis can be computed easily via

$$sphere \propto c_2^0, \quad 7.$$

$$cylinder \propto 2 \frac{(c_2^{-2})^2 - (c_2^2)^2}{\sqrt{(c_2^{-2})^2 + (c_2^2)^2}}, \quad 8.$$

$$axis = \frac{1}{2} \tan^{-1} \left(-\frac{c_2^{-2}}{c_2^2} \right). \quad 9.$$

As seen in the formulas above, the primary aberrations of the eye, sphere and cylinder, are described by the three lower order aberrations on the third row.

The higher order Zernike polynomials are needed to describe finer details in the structure of the wavefront. While many wavefronts from the eye can be resolved user lower order (5th and below) Zernike polynomials, small structures and discontinuities demand higher order Zernike polynomial terms.

A fine structure in a wavefront involves a subtle shift in the focal spot and demands a high quality lenslet array. If the focal spots are vaguely located it is impossible to accurately record minute differences across lenslets. Therefore, low density lenslet arrays cannot precisely resolve higher order aberrations. Errors in the spot locations cannot be overcome by using only Zernike polynomial fitting. Since the slopes are generally underpredicted with a low resolution lenslet, an fitting error caused by loss of higher spatial resolution will result in errors in the Zernike fit.

Certainly, ambiguous focal spots will destroy information about wavefront details and it will also degrade the measurement accuracy of the primary aberrations sphere and cylinder. The true danger is that there is often no obvious signal to the user that the data is inaccurate. To explore how lenslet resolution affects the zonal reconstructor, we considered the case of a pure Zernike polynomial Z₅⁵ as a simulation of an ocular wavefront. The results are shown below in figure 4.2.

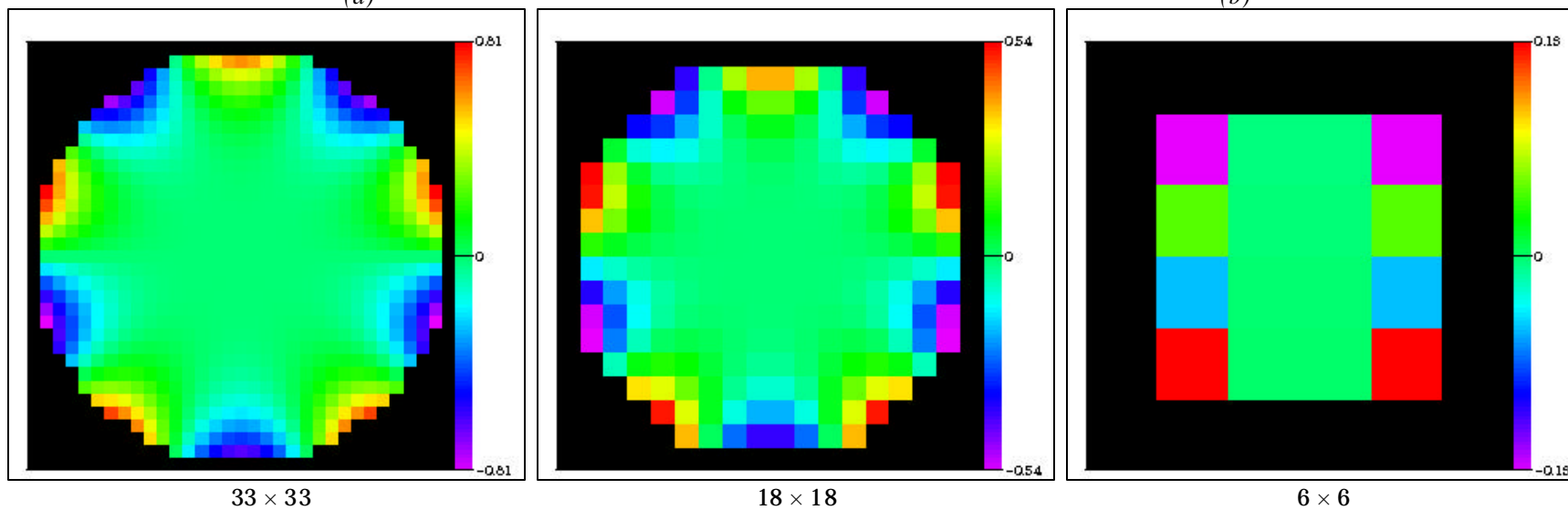
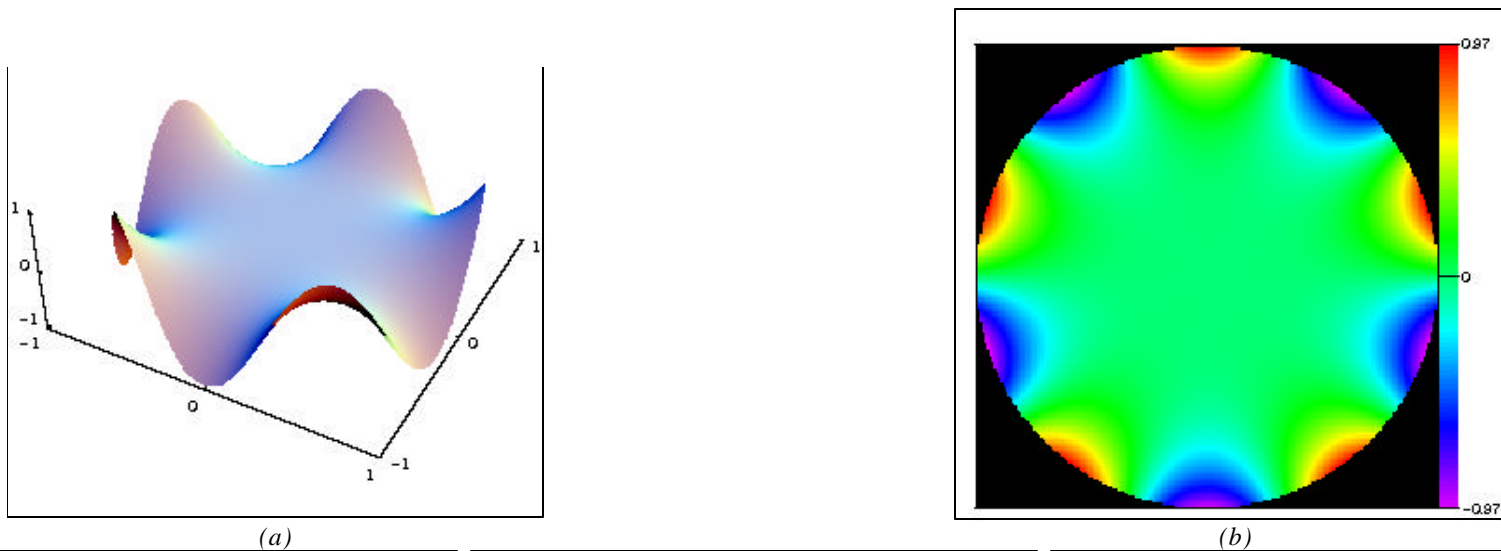


Figure 4.2: A pure Zernike polynomial viewed through three different lenslet arrays. The top row shows the input wavefront: figure (a) is the wavefront exiting the eye; figure (b) shows how the wavefront would be resolved by a lenslet array with unlimited resolution. The lower row compares the output from three lenslet arrays. Many RK patients have wavefronts similar to this one.

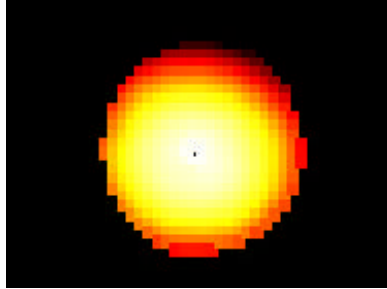


Figure 4.3 Wavefront (OPD) map from a normal eye. This image is the result of a Modal reconstruction to 4th order. The Zonal wavefront map is identical on this scale. The patients refraction was $-3.75 -1.00 \times 16$. The pupil diameter was 4.6 mm. The total P-V is $16.3 \mu\text{m}$.

For this simulation, we considered three lenslet arrays: the 33×33 array in COAS (785 sample points), an 18×18 array (216 sample points) and a crude 6×6 array (4 sample points). We used exact focal spot location and perfect reconstruction. Starting with known exact focal spot locations ignores the significant problem of finding the focal spots in the low density cases. So even though the lower density results look bad, they are actually better than would be achieved in practice.

The top row shows the input wavefront. The bottom row presents the OPD maps from zonal reconstruction. Compare these maps to the OPD map in the top row. The Zernike polynomial case is a simulation of a measurement of an eye that was treated with Radial Keratotomy. Clearly the first two cases are able to pick up the essential features of the wavefront. However, with extremely low resolution, the essential information is lost. Even though we have fit the data with an appropriate 4th order Zernike polynomial, there is not sufficient resolution to adequately present the data. While the Zernike polynomials could be used as interpolating functions, they would not present an accurate measurement of the input wavefront. The assertion that low density arrays can precisely measure sphere and cylinder is dubious. The belief that such lenslet arrays can make reliable measurements of the higher order aberrations in the eye is illusory.

Consider now the case of a real eye, measured with an ocular wavefront analysis system. In Figure 3.4, we present the results of a measurement with the COAS wavefront analysis system. This measurement is a Zernike reconstruction of the measured wavefront for an eye with -3.75 d sphere -1.00 d cylinder at 16° axis. Figure 3.3 does not include the zonal reconstruction for this case, since it appears exactly identical, differences being impossible to detect on the scale as presented. Certainly the wavefront map is adequate as presented, if we include the full sphere and cylinder in the depiction. However, once these terms are removed, then the higher order information becomes more apparent. These results are shown in Figure 4.4. For a normal eye, these depictions are usually adequate.

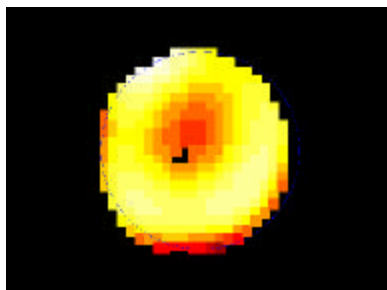


Figure 4.4 Higher order wavefront (OPD) map from a normal eye. This image is the result of a Modal reconstruction to 4th order with the first and second order terms subtracted. The total P-V (black to white on the color scale) is $1.04 \mu\text{m}$.

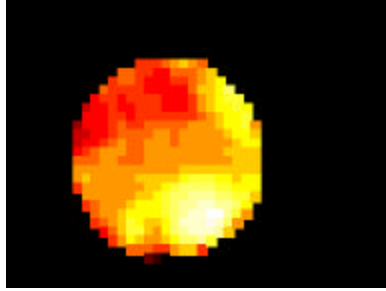


Figure 4.5 Zonal reconstruction with 2nd order terms subtracted from a normal eye. This image is the result of a Zonal reconstruction to 4th order with the first and second order terms subtracted. The total P-V (black to white on the color scale) is 1.9 μm .

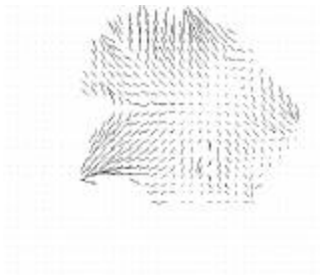


Figure 4.6 Vector slope map for an RK patient with poor outcome. This image shows the point by point slope measurement across the pupil. There are regions near the edges where no measurement was obtained. In these locations the scattering of the corneal was so strong that no light reached the wavefront sensor.

However, even for a normal eye there is structure that has higher resolution. In Figure 4.5, the same eye was measured using the Zonal reconstructor, with the second order terms (sphere and cylinder) subtracted from the results of the modal reconstructor. In this case much higher resolution information is obtained. The 4th order reconstructor, while it picks up most of the essential information, produced a total wavefront peak-to-valley that is almost $\frac{1}{2}$ of the zonal reconstruction value. This is because the highest point occurs in a narrow island.

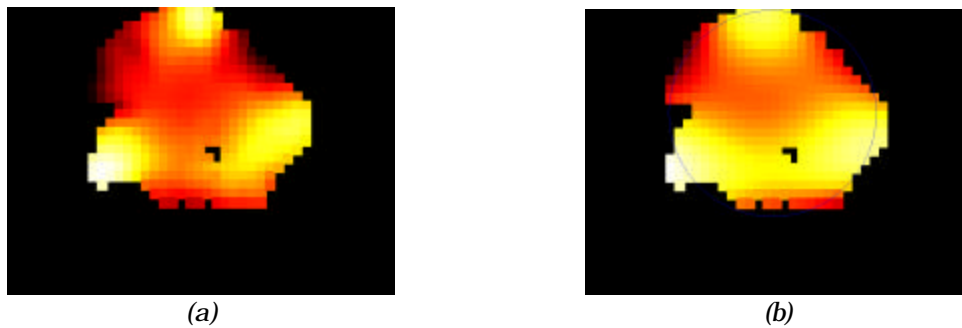


Figure 4.7 Wavefront map for an RK patient with poor outcome. Figure (a) is the result of a zonal reconstruction with 2nd order terms removed. Figure (b) shows the same data analyzed with the modal 4th order Zernike fit.

If we only had to measure normal eyes, there might be no need to ever view higher resolution information. The 4th or 5th order Zernike fits would provide adequate information, and the direct, quantitative comparisons afforded provide and added convenience. However, one of the key advantages to a ocular wavefront analyzer system, is that it allows us to measure pathologies in the ocular system. This is really the case we need the additional

information for anyway. So for diagnosis of kerataconus, dry-eye, investigation of corneal damage or edema, and for screening and measurement for laser vision correction surgery, the information is essential. Without the additional information, we may very well be causing more problems than we correct.

As an example of a pathological case, consider the poor outcome RK patient whose images were presented previously. The slope map itself is extremely interesting, with the deformations due to the radial cuts clearly evident in the image (Figure 4.6). In this case the slope of the wavefront deformation was so bad near the edges, that the light was scattered so strongly that it did not reach the wavefront sensor camera. Similarly, light from these regions would not be focused by the eye onto the retina. The wavefront map (with sphere and cylinder subtracted) is presented in Figure 4.7. There are three high regions near the edges. This patient has a lot of residual correction, and has poor BCVA. His night vision is even worse. While this is a somewhat extreme case, it is no more so than a kerataconus patient, or a slipped flap LASIK. Clearly the high resolution is needed to observe the important phenomena.

5. Dynamic range

With the proper design of the lenslet array, it is possible to exercise a great deal of control over the dynamic range of the wavefront sensor. It is easily possible to have both high lenslet density and high dynamic range.

The image projected by the lenslet array onto the CCD array is a pattern of spots. A snippet of the CCD image is shown on the right in figure 2.1. The spots are separated by the distance d . To be readily identified, these spots must be separate and distinct. A rule of thumb is that the size of the central spot r must be less than the spot separation d . In figure 5.1 (b), r is the distance from the maximum to the first minimum. For a square lens

$$r = \frac{f\lambda}{d} \quad 10.$$

where λ is the wavelength of the incident light.

The Fresnel number N_{Fr} is used to characterize the lenslet array and is defined as

$$N_{Fr} \equiv \frac{d}{r}. \quad 11.$$

For the case of the square lens the Fresnel number can be written as

$$N_{Fr} = \frac{d^2}{f\lambda}. \quad 12.$$

To preclude the focal spots from overlapping, the Fresnel number must be greater than two. In COAS, the Fresnel number of eight was selected to give a good dynamic range, while still producing focal spots that covered several pixels of the camera.

The dynamic range of a Shack-Hartmann wavefront sensor can be defined as the limiting travel of the focal spot such that the edge of the spot touches the projected lenslet boundary. This dynamic range q_{\max} is given by

$$q_{\max} = \frac{\frac{d}{2} - r}{f} = \left(\frac{N_{Fr}}{2} - 1 \right) \frac{\lambda}{d}. \quad 13.$$

The limited dynamic range depends upon the maximum angle that can be measured by a single lenslet, as well as the total number of lenslets. Over a single lenslet, the maximum wavefront is given by:

$$W_{\max, l} = q_{\max} d \quad 14.$$

The maximum wavefront that can be measured depends upon the type of wavefront aberration, and the maximum wavefront per lenslet. For tilt the maximum wavefront over the whole aperture is $W_{\max, l} \times N_l$. For a wavefront with aberration of Zernike order n : the maximum wavefront error is given by:

$$W_{\max} = \frac{N_{Fr} N_l I}{4n}. \quad 15.$$

Thus higher Fresnel number and larger number of lenslets increase the maximum wavefront error that can be measured. Both of these are the result of designing a lenslet with high resolution. While it may seem that a very short focal length lens would be useful (high Fresnel number), in this case the number of pixels that are covered by the focal spot is greatly reduced. This reduces the accuracy of the measurement.

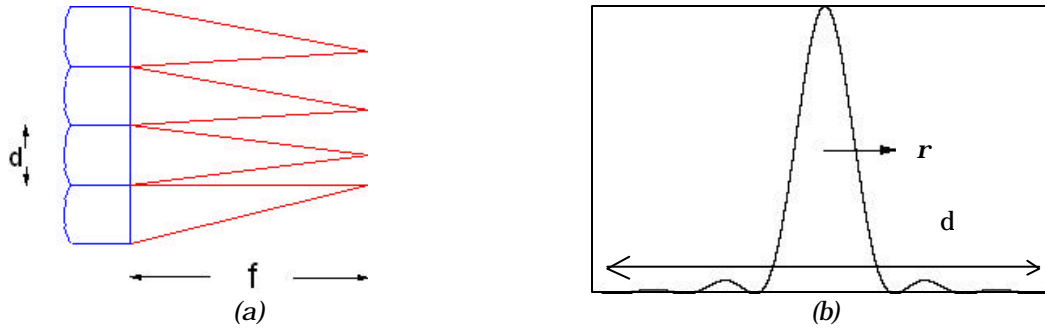


Figure 5.1 Basic parameters in lenslet design. Figure (a) Shows a cross section of four lenslets and their focal spots. Figure (b) shows the intensity profile for a single focal spot.

6. Conclusions

We have explored the development of high resolution ophthalmic wavefront sensor systems. For accurate results that are useful for measurement of pathologies, high resolution wavefront sensors have been shown to have advantages. For accurately find the locations of the focal spots, the size of the lenslet must be fine enough that the wavefront is essentially planar across the sample region. If the wavefront is not planar over the sampled region, then the focal spot will blur and it will be difficult to locate its position. Error in the location of the focal spot translates to error in reconstructing the wavefront. Such error will destroy the ability to resolve higher order aberrations and learn about the finer structure of the eye.

Smaller lenses do not necessarily have a smaller dynamic range; the lenslet design can be adjusted to expand the dynamic range of the device. In fact, with smaller lenslets there are more samples across the measurement region. Usually this leads to more dynamic range, not less.

Of course dividing a beam into smaller portions means there is less light in each portion. For measurements of the human eye, this has not caused any problems, because the required amount of light is still well within acceptable limits. COAS illuminates the eye with roughly 10% of the maximum power recommended in ANSI Z 136.1 (1993) and this had proven adequate. So even if some pathology were found that required a significant increase in illumination the input light level could be quadrupled comfortably.

7. References

- ¹ T. O. Salmon, L. N. Thibos and A. Bradley, "Comparison of the eye's wave-front aberration measured psychophysically and with the Shack-Hartmann wave-front sensor," *J. Opt. Soc. Am A*, 15 (9), pp. 2457–2465 (1998).
- ² J. Liang, B. Grimm, S. Goelz, and J. F. Bille, "Objective measurement of the wave aberrations of the human eye with the use of a Hartmann-Shack wave-front sensor," *J. Opt. Soc. Am. A* 11, 1949–1957 (1994).
- ³ J. Liang, D. R. Williams, and D. T. Miller, "Supernormal vision and high-resolution retinal imaging through adaptive optics," *J. Opt. Soc. Am. A* 14, 2884–2892 (1997).

⁴ S. Panagopoulou, "Correction of high order aberrations using WASCA in LASIK for myopia," Fall World Refractive Surgery Symposium, Dallas, TX, October 19–21, 2000.

⁵ D. R. Neal, W. J. Alford, and J. K. Gruetzner, "Amplitude and phase beam characterization using a two-dimensional wavefront sensor," SPIE 2870, pp. 72–82 (1996).

⁶ D. R. Neal, D. J. Armstrong and W. T. Turner, "Wavefront sensors for control and process monitoring in optics manufacture," SPIE 2993 (1997).

⁷ Born, M. and Wolf, E., Principles of Optics 7e, Cambridge University Press, 1999.

⁸ Southwell, W., Wave-front estimation from wave-front slope measurements, J. Opt. Soc. Am., Vol. 70, No. 8, 8/1980.

⁹ Thibos, L., Applegate, R., Schwiegerling, J., and Webb, R., Standards for Reporting the Optical Aberrations of Eyes, available at <http://www.osa.org/Homes/vision>.